

-ITEP-51-94



INSTITUTE OF THEORETICAL
AND EXPERIMENTAL PHYSICS
FERMILAB

MAR 9 1994 51-94

IBRAP

D. Yu. Akinov, A. I. Bolozdynya, A. D. Brastilov, A. A. Burenkov,
A. Chen, D. L. Churakov, V. F. Kuzichev, R. A. Minakova, T. A. Osipova,
I. A. Rogovsky, G. A. Safronov, V. M. Shershukov, S. A. Simonychev,
V. N. Solovov, G. N. Svirnev, M. M. Smolin, V. P. Tchernyshev,
W. Turchinets

LIQUID XENON/KRYPTON SCINTILLATING CALORIMETER

Submitted to NIM

MOSCOW 1994

LIQUID XENON/KRIPRON SCINTILLATING CALORIMETER: Preprint ITEP 94-51/

D.Yu. Akimov, A.I. Bolosdynya - M., 1994 - 29p.

A scintillating LXe/LKr electromagnetic calorimeter has been built at the ITEP and tested at the BATES (MIT) accelerator. The detector consists of PMT matrix and 48 light collecting cells made of aluminized 50 microns Mylar partially covered with p-terphenyle as a wavelength-shifter (WLS). Each pyramidal cell has $(2.1 \times 2.1) \times 40 \times (4.15 \times 4.15)$ cm dimensions and is viewed by FEU-89 glass-window photomultiplier.

The detector has been exposed at 106-348 MeV electron beam. The energy resolution $\sigma_E/E \approx 3\%/\sqrt{E}$ at 100-350 MeV range in LXe, the coordinate resolution $\sigma_x \approx 0.7$ cm, the time resolution for single cell $\sigma_t \approx 0.6$ ns have been obtained.

Possible ways to improve energy resolution are discussed.

Fig.-13, ref.-8

1. INTRODUCTION.

LXe/LKr electromagnetic calorimeters are proposed as precise, fast, radiation stable devices for accelerators of a new generation [1,2]. Some recent attempts to build LXe scintillating calorimeter were not successful because of difficulties of effective UV light collection (150 nm for Kr and 170nm for Xe) [3,4]. Standard approach needs UV sensitive photodetectors, high effective UV reflectors and extrimely UV-transparent scintillating liquids. Simulations show even 1m attenuation length achieved in laboratories is not enough to reach precise resolution. Our approach is based on using of visible light sensitive PMT and aluminized Mylar reflector covered with wavelength-shifter (WLS) to shift scintillating spectrum at the visible range. On this way we found desirable response functions can be obtained for calorimeter cell of a needed size [5].

The scintillating calorimeter LIDER (Liquid Detector for Electromagnetic Radiation) has been built and was previously tested at ITEP with LKr as a working medium [6]. The calorimeter has been investigated in detail at the BATES (MIT) electron accelerator with LXe filling.

2. EXPERIMENTAL SET-UP.

The scintillating calorimeter LIDER (Fig.1) consists of cellular Mylar reflector structure viewed with matrix of photomultipliers immersed in a liquid noble gas. The photomultipliers are divided in 5 groups (7 to 11 PMTs per group). Each group is power supplied by common active divider placed outside of the cryostat. The electrical inputs are coming through multipin metal-glass feedthroughs. Vessel with liquid (A, fig.1) is placed inside the cryostat including three jackets: (B) filled with nitrogen gas, (C) filled with liquid nitrogen, (D) vacuum isolation. Aluminium supplementors surround the reflector structure to reduce used volume of LXe to 35 liters. The heaters (3) provide thermostabilization with $\pm 0.5K$ accuracy. The temperature is measured by copper-constantan thermocouples. The LIDER is placed on a moving remote-controlled table at the BATES electron beam.

The reflector structure is glued from 45 pyramidal light-collecting cells (Fig.2). Each cell of $(2.1 \times 2.1) \times 40 \times (4.15 \times 4.15)$ cm dimensions is made of 50 μm aluminized Mylar strip-like covered with p-terphenyle. One strip per wall picturing is chosen for home-made reflector structure. The shape of p-terphenyle strips is experimentally found to reach uniformity of light collection along a cell; it has been shown the response functions are similar as for LKr and for LXe fillings in the same cell [5]. The longitudinal response functions for two different cells filled by LKr is shown in Fig.3 which demonstrates good reproducibility of response function for found WLS-picturing. Transversal response function is Monte-Carlo simulated (fig.4a).

Some types of PMT were tested specially to be used in LKr/LXe. Photomultiplier FEU-85 (table 1) has demonstrated the best properties: a magnitude of signals does not depend on temperature; noise of PMT at the LKr temperature is 2 times lower

than noise of PMT at the room temperature; it is mechanically stable up to 10 atm. extra pressure.

The ^{237}Pu implanted into Mylar α -sources ($1 \times 1 \text{ mm}^2$ area) of 10-100 decays per second activity are placed in some cells

- to test a uniformity of light-collection,
- to calibrate a spectrometric channel,
- to test a LXe/LKr transparency,
- to determine a position of a liquid level during of filling of the detector.

Each spectrometric channel is also controlled by pulse nitrogen laser (333 nm). Laser radiation activates the plastic scintillator (12). The scintillating light passes as to each PMT through plastic fiber (13) and to the monitoring photomultiplier (14). Stability of PMT in time is measured by comparison of signals from each cell and from the monitoring PMT. Variation of signal magnitude of $<2\%$ was found for FEU-85 during run (7 hours) in LXe.

The gas system is shown in Fig.5. Cooled stainless 40 liters high pressure cylinders (BPC) are used for Xe gas storage. Xenon was purified in a gas phase passing through the "Oxysorb", "Monotor" and "Hydrox-801" purifiers during of the LIDER filling. UV transparency of LXe is measured in 1 liter control chamber with PM tube and two α -source placed at different distances from PMT-window covered by p-terphenyle. Liquid Xenon taken from the LIDER after beam tests has demonstrated attenuation length of 3 cm at purification by means of "Monotor" + "Hydrox-801" and of 5 cm at purification by means of "Oxysorb" + "Monotor" + "Hydrox-801".

The read-out system is based on CAMAC electronics and IBM/PC-486 computer (Fig.6). Data acquisition and ON-LINE data processing are provided by the MES programm [7]. The 5 ms "dead" time of the readout system is defined by the acquisition time and ON-LINE processing time of the computer. A special electronic

system is used to protect of pile-up effect. The 150 ns gate is used because of 95% of scintillation light is collected for this time (Fig.7). The 2048 channels (11 bits) CDC LeGroy 4300B FERA are used for PMT pulse digitizing. The mean magnitude of signals from central cell corresponds to about 500-1000 channels of CDC (200 keV per channel). The signals from the beam counters CE1 and CE2, muon counters CM1 and CM2, and laser calibration counter CL are also digitized. This information is recorded event by event to hard disk. OFF-LINE data treatment is carried out in VAX of MITLNS.

The triggers are generated with this system:

- 1) beam events (for electrons passing through CE1, CE2 counters; see fig.6),
- 2) pedestal events (from pulse generator),
- 3) α -events (5 independent triggers for one cell with α -source in each groupe),
- 4) muon events (CM1 and CM2 coincidence from cosmic muons),
- 5) laser events.

3. MONTE-CARLO SIMULATIONS.

Influence of the LIDER configuration on energy resolution is investigated with GEANT Monte-Carlo program. As fluctuation of energy deposited in entrance windows, in reflector walls, in other constructive elements and fluctuation of energy leakage out of the sensitive volume are taken in consideration. Longitudinal response function measured earlier [5] and transversal response function calculated specially (Fig.4) are included in the program.

Response functions for light collecting cells are simulated by the special Monte-Carlo program. The transparence of the liquid, mirror and diffusive reflective index for aluminized Mylar and p-terphenyl strips as for visible and for UV light are taken in consideration. Simulations show a response function are quite sensitive as to attenuation lenght in a liquid and the mirror

reflective index for UV light. LXe is considered to be transparent for visible light. The aluminized Mylar reflective index of 85% for visible light and 50% for UV at normal incident light are used for calculations. The last value has been measured with 170 nm UV source and UV-sensitive photomultiplier. The reflective indexes provide a quite good correspondence of the simulated longitudinal response function to the measured one [5] (Fig. 3). The WLS covered Mylar is considered as a total diffusive reflector with 70% efficiency for visible light and as a total absorber for UV light. The diffusive reflective index of 10% for aluminized Mylar is used as for visible and for UV light. The transversal response function is presented in Fig. 4 for 5 cm attenuation length of UV light in LXe.

The influence of leakage fluctuations on energy resolution is presented in Fig. 8. The curves are corresponded to fluctuations of energy deposited in the LIDER due to forward (1), backward and lateral (2) leakage fluctuations. Fluctuations of absorbed energy in "dead" matter of the Mylar walls ($2 \times 50 \mu\text{m}$) and possible "dead" LXe layer between cell walls (0.5 mm) and between the inner window and the reflector structure (5 mm) are shown by (3) and (4) curves. The (5) curve corresponds to fluctuation of the energy lost in the entrance windows (totally 3 mm of stainless steel). Comparison of the above simulations shows that energy resolution of the LIDER built with "ideal" cells (controlled by absolute uniform response functions) is limited generally by fluctuations of deposited energy in lateral direction at the 100-500 MeV energy range (1 curve, Fig. 8).

The Monte-Carlo calculated dependence of the LIDER detector energy resolution on electron beam energy is presented in Fig. 9. The curve 1 corresponds to detector with the "ideal" light collecting cells, curves 3 and 4 corresponds to detector with one-strip covering cells for 5 cm and for 3 cm attenuation length.

4. EXPERIMENTAL DATA.

The LIDER has been exposed at 106, 174.3, 260 and 348 MeV electron beams at the BATES accelerator. The time structure of the beam is the 15 μ s bunch consequence with 600 Hz repetition rate with intensity 0.5-2 electrons per bunch (300-1000 electrons per second).

4.1 Calibration procedure.

To obtain the calibration coefficients the central part of the LIDER (5x5 cells) has been scanned by beam with step of 20 mm.

Three calibration procedure are used. According to the first one the calibration coefficients for all cells are calculated by minimization of the energy distribution width. For this purpose the following function is minimized by means of MINUIT code:

$$F(k_1, \dots, k_M) = \sum_{i=1}^N (E_i - (E_0 - E_L)) ^2 / N,$$

where $E_i = \sum_{j=1}^M k_j A_{ij}$ is an energy for i-th event, k_j is a calibration coefficient for j-th channel, A_{ij} is a pulse amplitude for i-th events j-th channel, N is number of events, E_0 is the electron beam energy, E_L is a leakage energy. E_L depends on beam coordinates and it is calculated with GEANT simulation program. The procedure was checked for simulated events.

According to the second method two dimensional plots of energy deposited in the calorimeter outside the j-cell $\tilde{E}_{ij} = (E_i - e_{ij})$ on energy deposited in this cell $e_{ij} = k_j A_{ij}$ are draws for every j. For correct calibration coefficients all points on this plots must lie close to the $\tilde{E}_{ij} = (E_0 - E_L) - e_{ij}$ line with $\text{tg}(\alpha_j) = -1$. For noncorrect coefficients the experimental points

lie close to a line with $|\text{tg}(\alpha_j)| > 1$ if the coefficient is understated or $|\text{tg}(\alpha_j)| < 1$ if the coefficient is overstated. The coefficients are calculated with iterative procedure where the next iteration coefficients are defined by $k_j(\text{next}) = k_j \cdot \text{tg}(\alpha_j)$.

The third method is the following iterative procedure. Calibration coefficients are fitted to provide the measured energy of $(E_0 - E_L)$ independently on the position of shower center-of-gravity. If the energy is less (more) than $(E_0 - E_L)$ for events with shower center-of-gravity close to some cell then the appropriate coefficient in this cell is increased (decreased) in the next iteration.

The results of the above calibration procedures are adequate.

4.2 Energy characteristics.

The energy spectrum for 348 MeV electrons reconstructed with obtained calibration coefficients is shown in Fig.10. The experimental data on energy resolution for different electron energies are presented in Fig.9 (stars). The data for 106 MeV, 174.3 MeV, and 260 MeV electrons are measured with the detector filled with liquid Xenon purified in a gas phase by the "Monotor" and "Hydrox-801" purifiers (attenuation length for UV light measured in the control chamber is about 3 cm). The data for 348 MeV electrons was obtained with xenon purified additionally by "Oxisorb" purifier (attenuation length is about 5 cm).

Fig.11 shows the experimental and simulated dependences of the derivation from E_0 of the measured shower energy on the position of the shower center-of-gravity in X direction. Bumps on the last dependence correspond to the position of reflector walls and are result of nonideal transversal response function (Fig.4).

4.3 Coordinate characteristics.

Coordinates of an incident electron beam are defined as a

center-of-gravity position of the distribution for energy deposited in the detector. A spread of the beam position is determined by 0.5×0.5 cm scintillating counter. The X distribution of the center-of-gravities is presented in Fig.12, from which coordinate resolution of $\sigma_x \approx 0.7$ cm has been found taking into account the beam spread.

An ideal calorimeter should provide linear dependence of the shower center-of-gravity position on beam position. To investigate such dependence the calorimeter has been scanned by electron beam in X and Y directions with step of 5-10 mm. Fig.13 shows an ability of the LIDER to measure position of incident electron of 348 MeV as a calculated position of the shower center-of-gravity.

4.4 Time characteristics.

The TOF measurements were performed by means of LeCroy 2228A TDC at 174.3 MeV beam energy. A start signal for TDC is generated by the beam counter, a stop signal is generated by the cell with maximum deposited energy. The time resolution of $\sigma_T = 0.6$ ns (Fig.14) has been obtained taking in consideration the time resolution of the start beam counter. The total pulse duration (95% of charge) from a single cell is less than 150 ns (see fig.7) and is defined by decay time of scintillation.

5. DISCUSSION

The presented experimental data demonstrate good time properties, sufficiently good coordinate resolution of the detector and are agreed with Monte-Carlo simulations. The energy resolution is still 2.5 - 3 times worse than GEANT predicted for "ideal" light collection. It is caused by the transversal nonuniformity of "one-strip per wall" light-collecting structure. As the range of such nonuniformity and energy resolution are depended on LXe transparency (curve 1, Fig.15) if the attenuation

length is comparable to transversal dimensions of the cell (≈ 5 cm) only. Therefore the achieved parameters of the detector can not be essentially improved by means of increasing of LXe transparency.

Another way is to use more fine picturing which is much more expensive in manufacturing. Curve 2 in Fig.15 and curve 2 in Fig.9 demonstrate about 2 times better energy resolution for the detector with picturing of 4 WLS strips per wall of light collecting cell relatively to picturing with one-strip per wall.

Further improvement of resolution is possible using the cell with surface totally covered by transparent to visible light WLS (the p-terphenyle layer is diffusive reflector for reemitted light and partially absorbs it). Preliminary tests with cell covered with such WLS developed by Single Crystal Institute (Khar'kov) have shown only 10-15% transversal nonuniformity (near wall rise). The longitudinal uniformity can be achieved in this case by variation of WLS concentration along the cell. But a new WLS has to be investigated additionally for stability in liquids, radiation hardness and reproducibility of longitudinal uniformity for mass-produced cells.

Time characteristics of the calorimeter may be improved by adding a molecular dependant as N_2 in LXe to reduce decay time of long living component of scintillation.

6. CONCLUSION

The first full scale scintillating calorimeter has been built and tested. In LXe the measured energy resolution is $\sigma_E/E \approx 5\%/\sqrt{E}$. The developed method of "visible sensitive photodetector + Mylar reflector with WLS-covering" opens a real way to build precision calorimeters using non-expensive photo-detectors and demanded LXe purity easy to be achieved ($L_{att.} = 5-10$ cm).

Spatial resolution of the calorimeter $\sigma_x \approx 0.7$ cm for single

electron shower in LXe.

Good time properties - time resolution $\sigma_T \approx 0.6$ ns and utilized signal width of 150 ns - allow to use the detector at high luminosity accelerators for example in experiments for measurements of parity violating electron scattering on hydrogen [8].

ACKNOWLEDGEMENT

We thank for a great support from Prof. R.P. Redwine, Prof. S. Kowalski, Dr. L. Stinson, and others of MIT Laboratory for Nuclear Science and of the Bates Linear Accelerator Center during these investigations.

Table 1

General characteristics of FEU-85 photomultiplier.

Photocathode	semi-transparent head-on SbCsI useful diameter of 25 mm
Spectral sensitivity range	300-600 nm
Maximum spectral sensitivity	340-440 nm
Luminous sensitivity	78 $\mu\text{A}/\text{lm}$
Number of stages	11
Tube diameter	30 mm
Maximum length	110 mm
Mass	50 g
Lifetime	2000 h

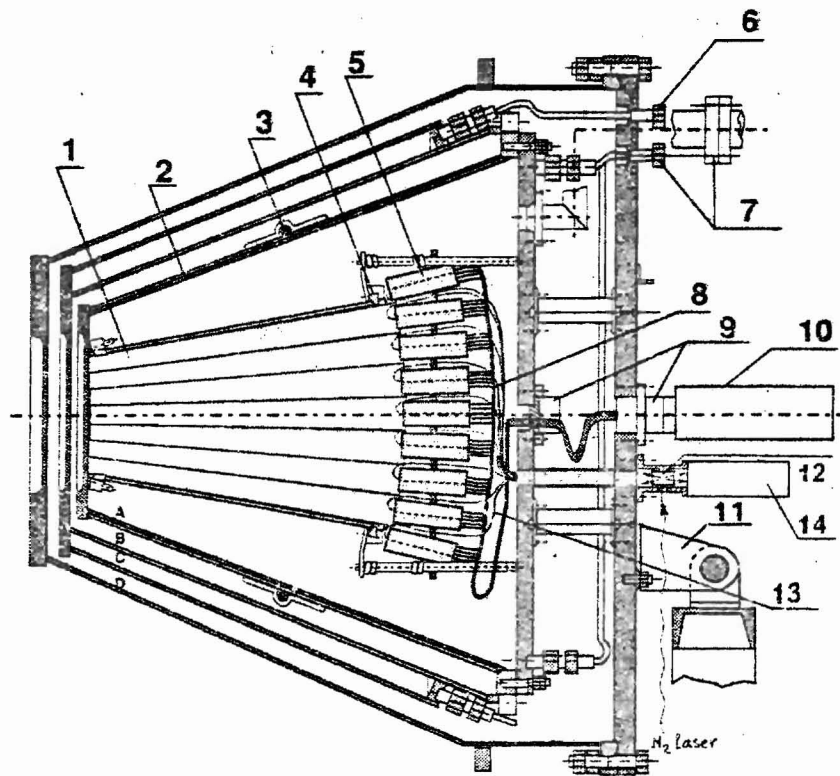
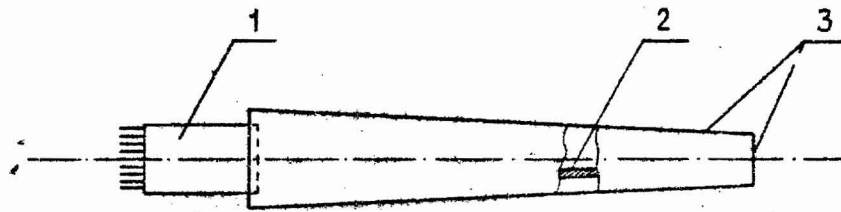
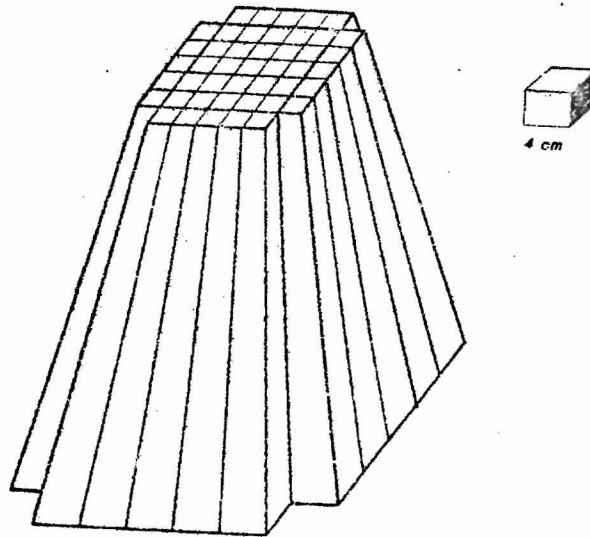


Fig.1. Schematic drawing of LKr/LXe scintillating calorimeter:
 1-Mylar reflector, 2 - LKr/LXe vessel, 3 - heater, 4 - support
 for Mylar reflector, 5 - PMT in magnetic screen, 6 - liquid
 nitrogen input, 7 - Kr/Xe gas input, 8 - PMT connectors, 9 -
 multipin metal-glass feedthroughs, 10 - PMT divider, 11 -
 support, 12 -plastic scintillator, 13 - fiber, 14 - monitoring
 photomultiplier,

- a - LKr/LXe volume,
- b - gas jacket,
- c - liquid nitrogen jacket,
- d - vacuum isolation



a



b

Fig.2. Single calorimeter cell (a) : 1 - PMT, 2 - fragment of p-terphenyle strip, 3 - Mylar pyromidal reflector; and reflector structure (b).

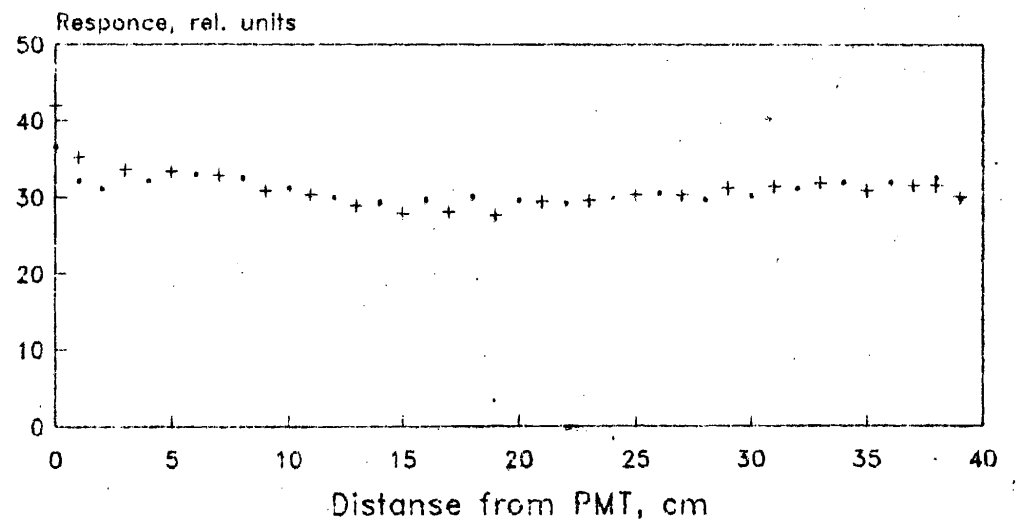


Fig.3. Longitudinal response function measured for two different reflector cells.

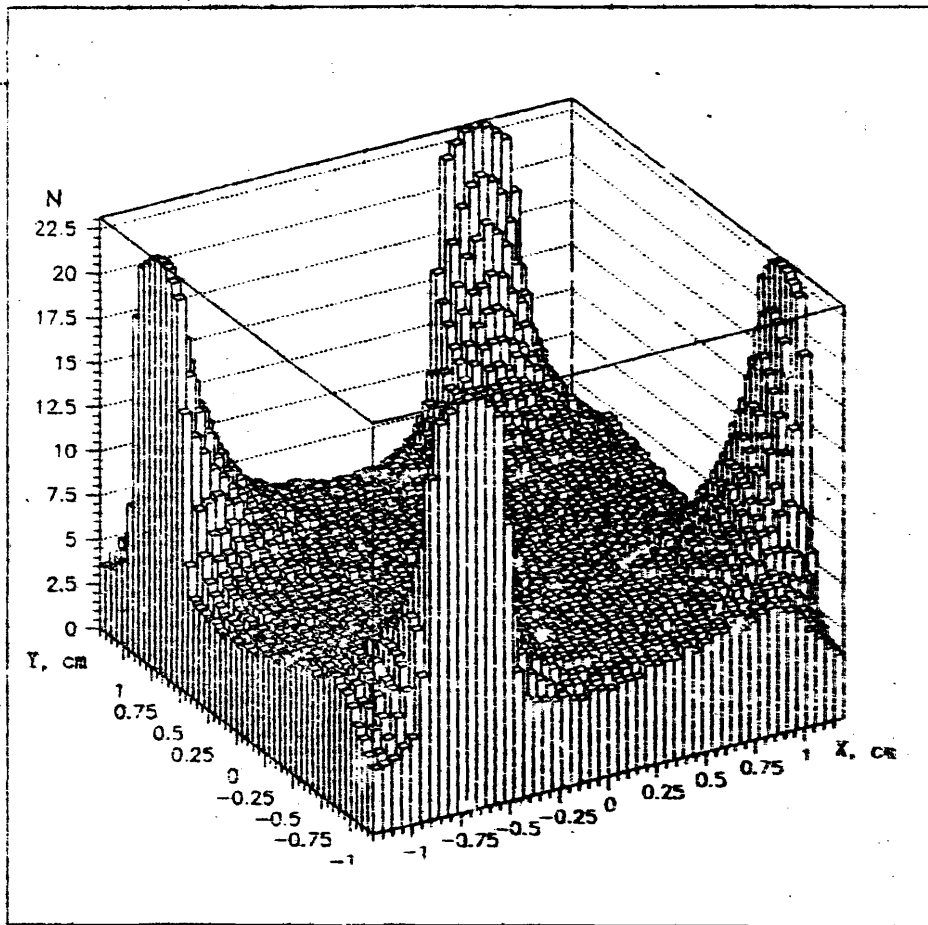


Fig. 4a. Transversal response function N simulated for 50% UV reflective index and UV attenuation length of 5 cm for one strip per wall covering

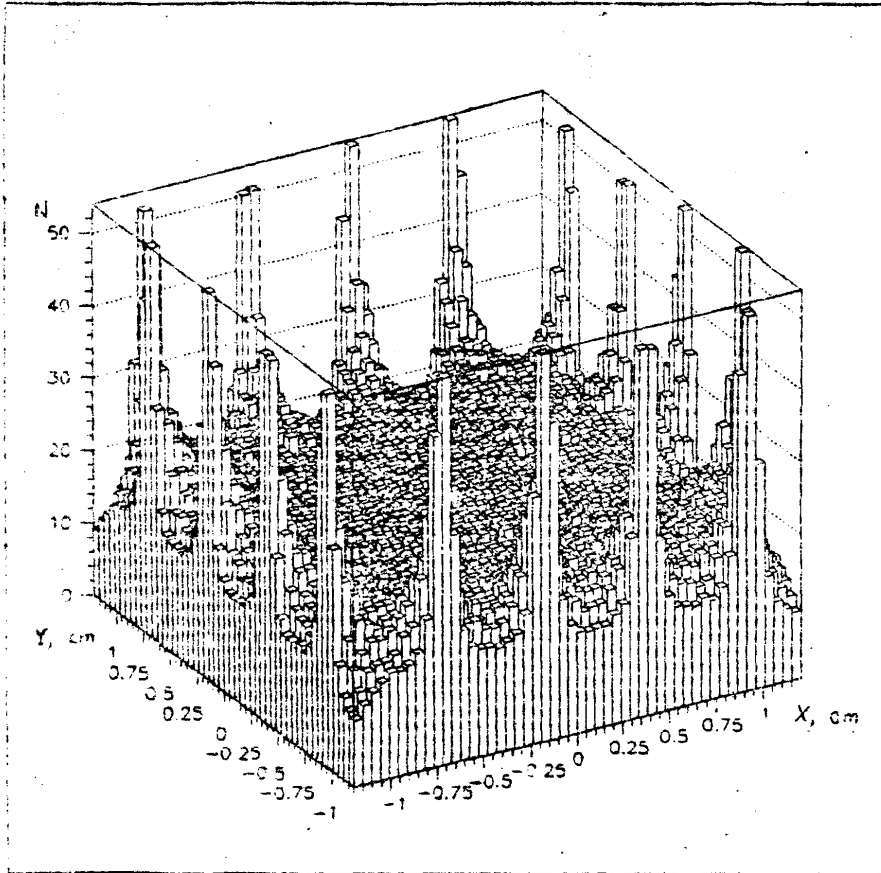


Fig. 4b. Transversal response function MC simulated for 80% UV reflective index and UV attenuation length of 5 cm for four strips per wall covering

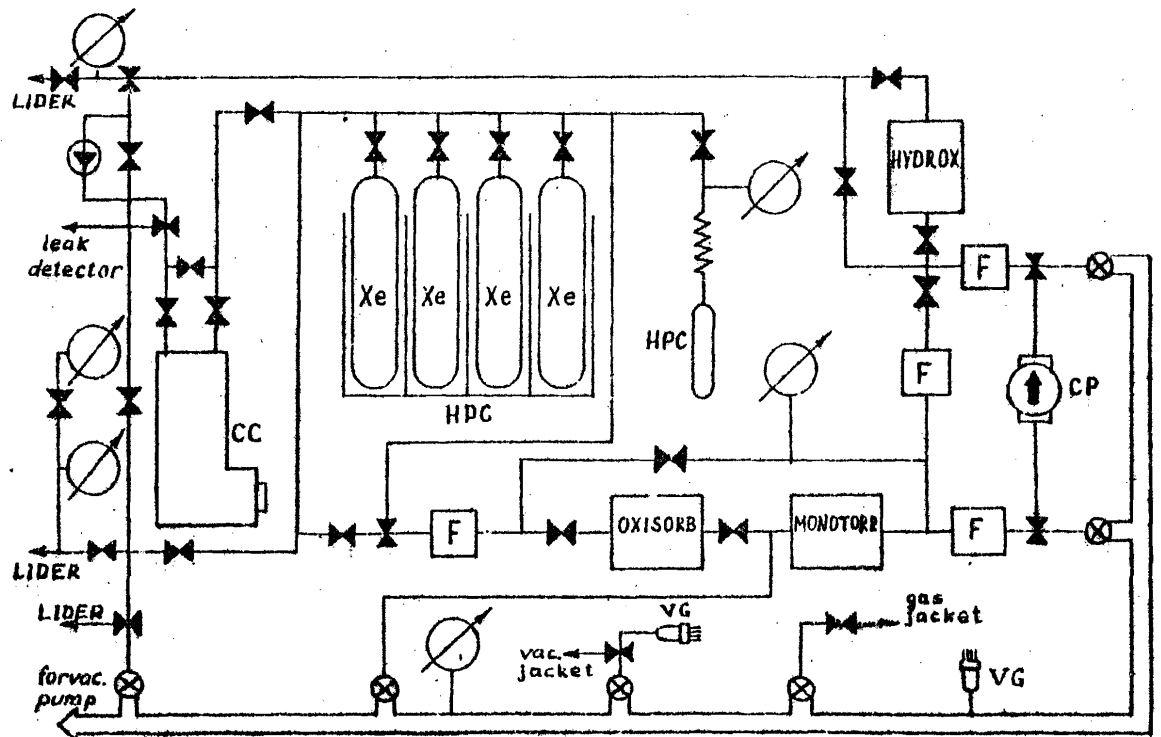


Fig.5. Gas system: CC - control chamber, HPC - high pressure cylinders, F - gas filters, CP - circulating pump, VG - vacuum gauge.

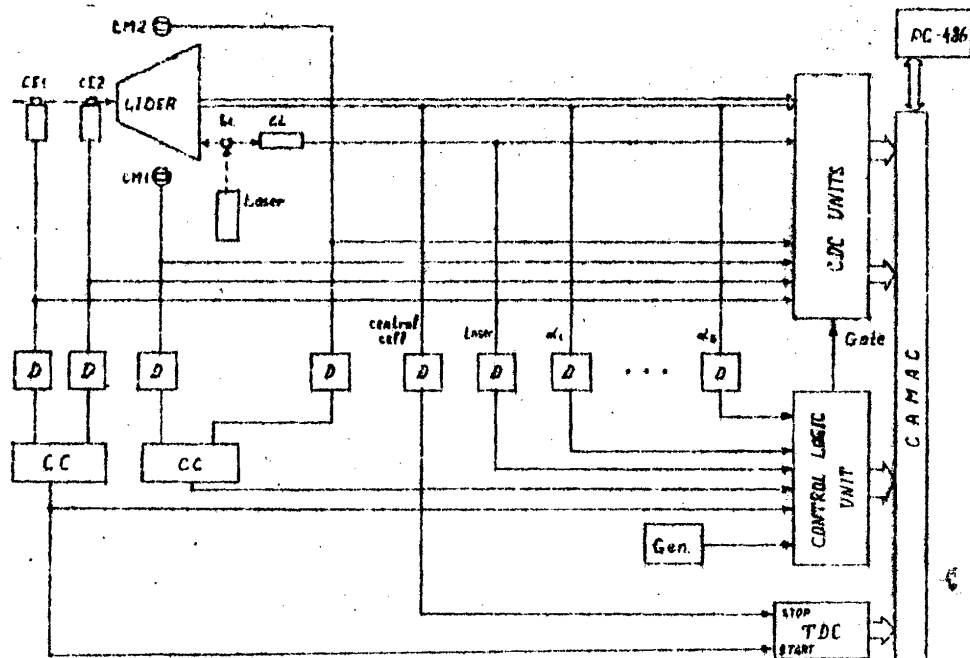
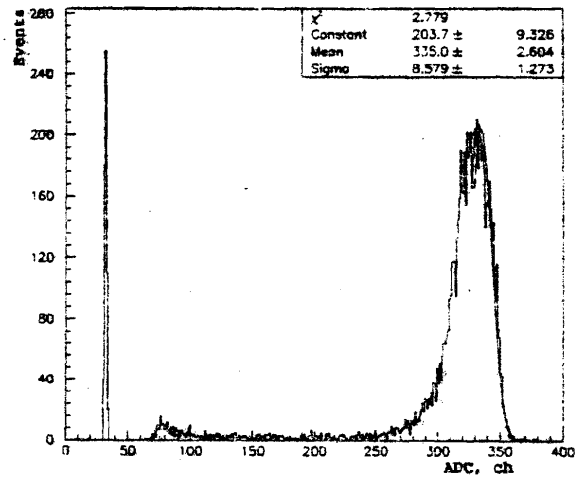


Fig.6. Read-out electronics: CE1,CE2 - beam counters, CM1,CM2 - muon counters, Sc. - scintillator, CL - laser pulse counter, D - shaper-discriminator, CC - coincidence circuits, Gen. - pulse generator, CDC UNITS - units of charge-to-digital converter LeCroy 4300B FERA, TDC - unit of time-to-digital converter LeCroy 2228A.



IA1
50 ns 20 mV

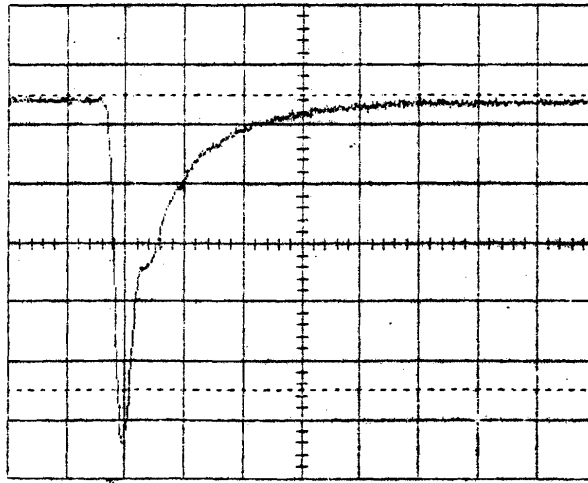


Fig.7. Scintillation signal from FEU-85 PMT covered by WLS in LXe activated by α -particles (pictured by digital scope) (a) and suitable pulse spectrum (b).

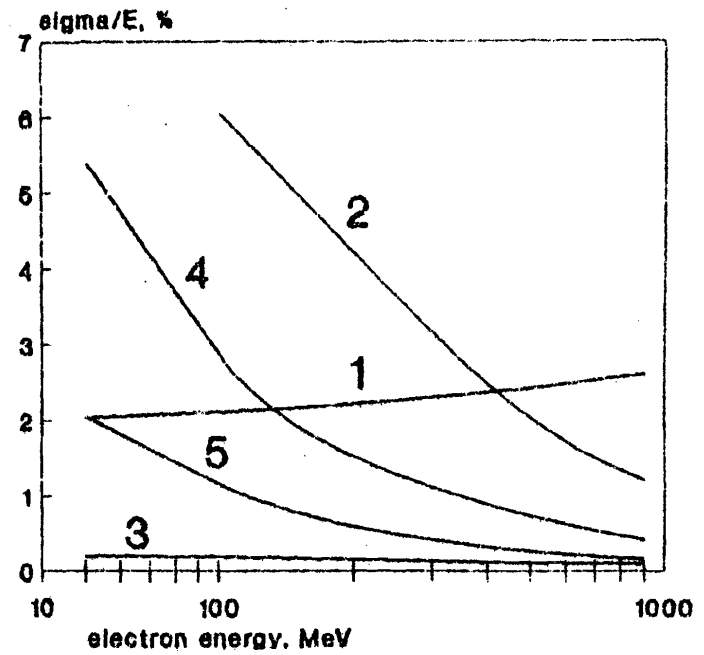


Fig.8. Dependence of fluctuation of energy deposited in the LIDER due to energy leakages in forward (1), backward and lateral (2) directions and due to absorption of energy in Mylar walls (3), LXe layer in front of the reflector structure (4) and in the inner windows (5) on energy of electron beam.

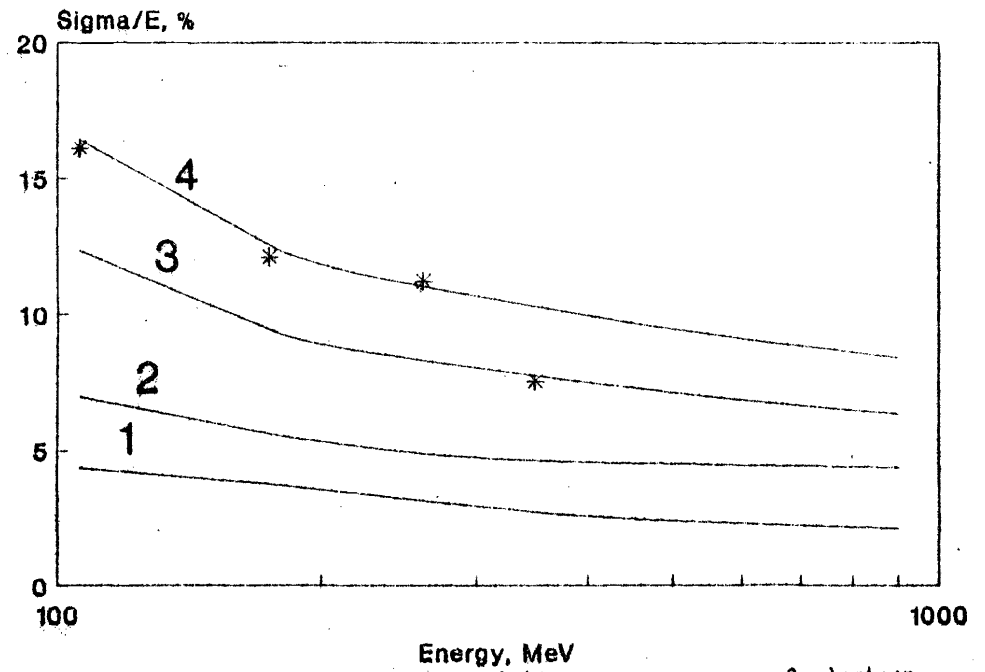


Fig. 9. Dependence of energy resolution versus energy of electron beam. Stars - experimental points. Curves: 1 - "ideal" cell, 2 - cell with four strips per wall picturing ($L_{att} = 5$ cm), 3 and 4 - cell with one strip per wall picturing with $L_{att} = 5$ cm and $L_{att} = 3$ cm correspondently.

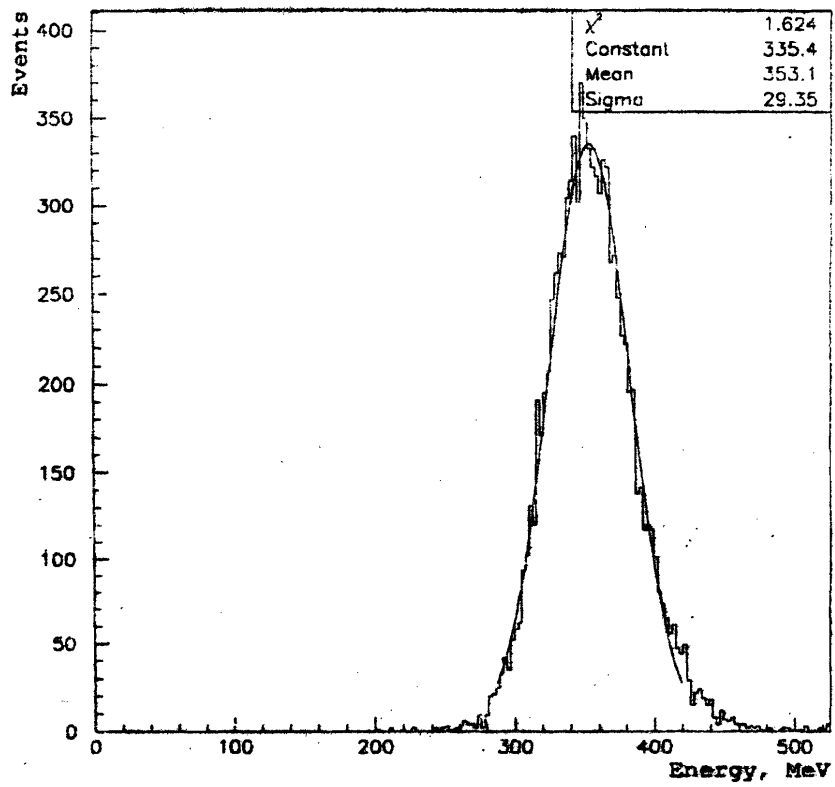


Fig.10. The energy distribution for 348 MeV electrons measured in the LIDER.

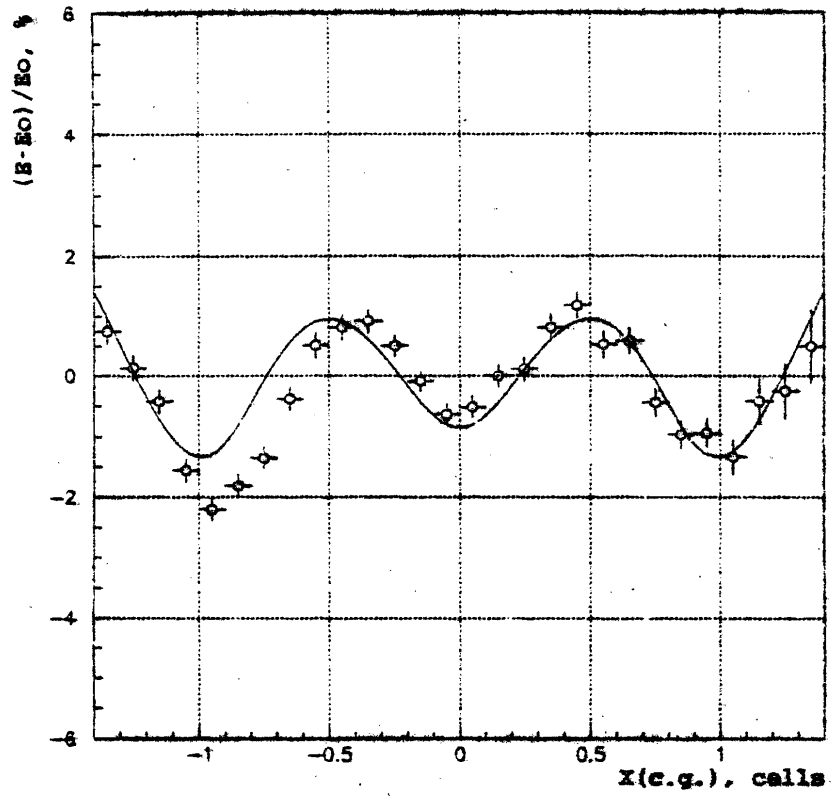


Fig.11. Dependence of the derivation of the shower energy from E_0 on the position of the shower center-of-gravity in X direction.

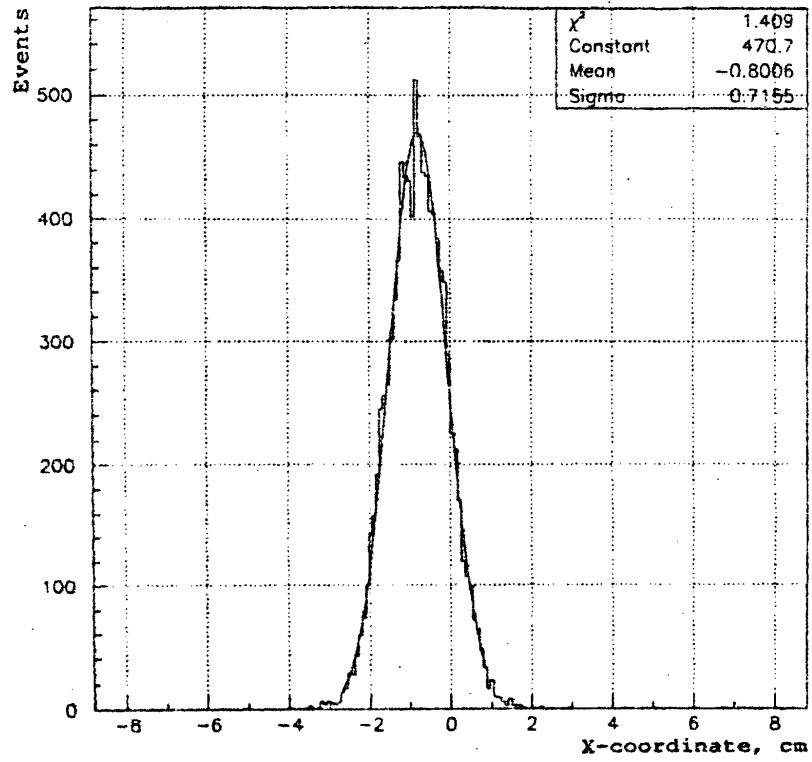


Fig. 12. The X-distribution of centers of gravity for 348 MeV beam energy.

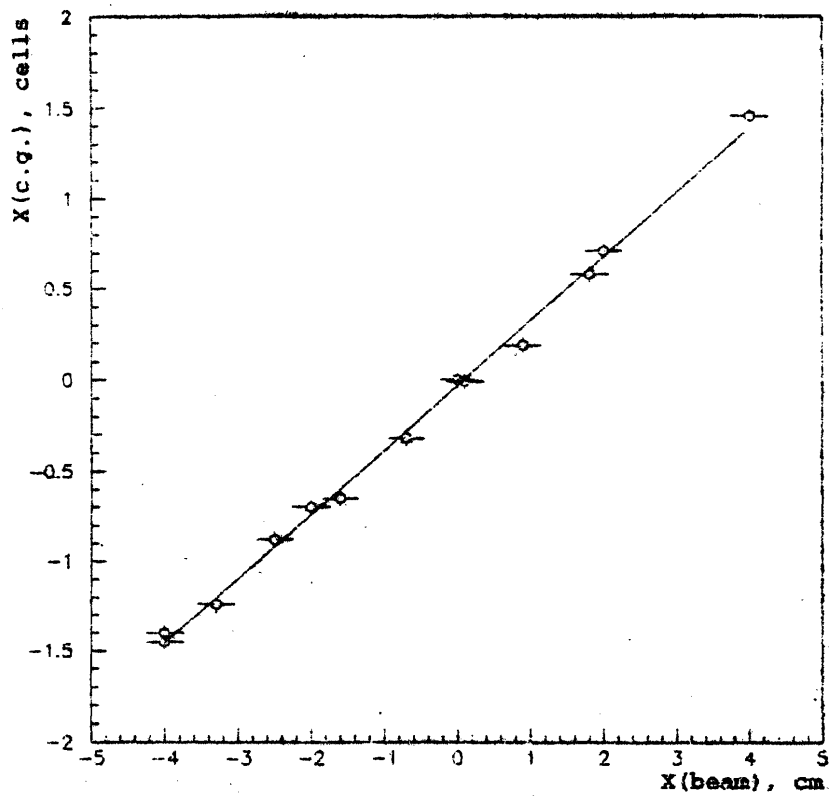


Fig.13. Dependence of position of the shower center-of-gravity on the beam position.

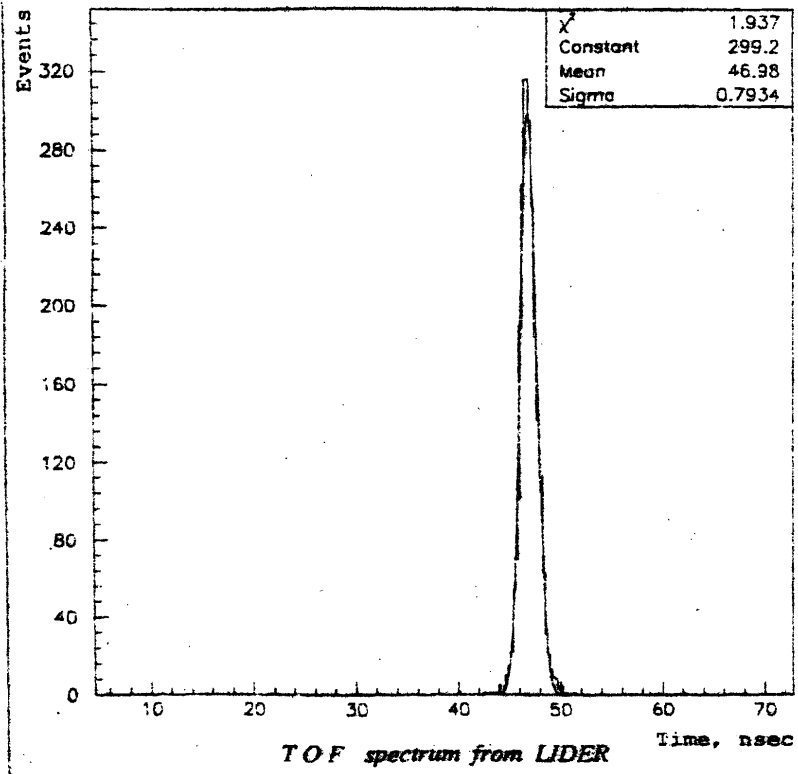


Fig.14. Time-of-flight spectrum for 174.3 MeV beam energy.

En.resolution via transparency dependece (Calculations for 50% UV refiact.coef.)

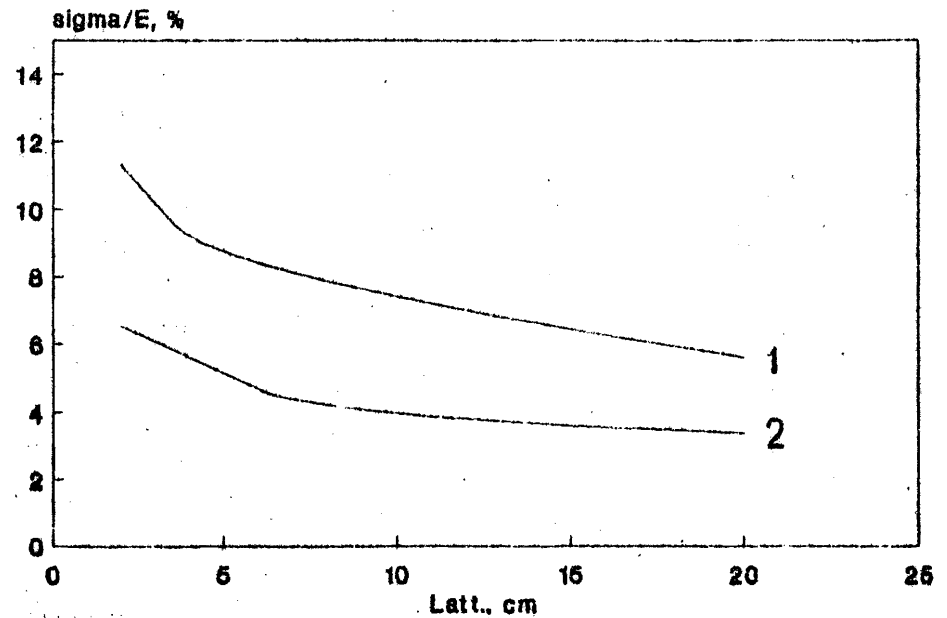


Fig.15 Simulated dependence of the energy resolution of the LIDER on the LXe attenuation length for reflector built of cells with one WLS-strip per wall picturing (1) , and of cells with four WLS-strips per wall picturing (2) at 348 MeV electrons.

REFERENCES

1. M.Chen e.a. Homogeneous scintillating LKr/LXe calorimeters// Nucl.Instr.and Meth. 1993. Vol.A327, P.187-192.
2. E.Radermacher, D.Schinzel, M.Chen, T.Doke, and S.Sugimoto. Liquid Detectors for Precision Calorimetry// In "Instrumentation in High Energy Physics, Ed.F.Sauli". Singapur: World Scientific Publishing Co., 1992. P.387-512.
3. A.Braem e.a. Observation of the UV scintillation light from high energy electron showers in liquid xenon// Nucl.Instr.and Meth. 1992. Vol.A320, P.228-237.
4. J.Seguilot,G.Passardy,J.Tischhauser and T.Ypsilantis. Liquid xenon ionization and scintillation studies for a totally active-vector electromagnetic calorimeter// Nucl.Instr.and Meth. 1992. Vol.A323, P.583-600.
5. D.Akimov e.a. Uniformity of a 37 cm long cell for LXe/LKr scintillating calorimeters// Nucl.Instr.and Meth. 1993. Vol.A333, P.618-621.
6. D.Akimov e.a. LKr scintillating calorimeter. M., Preprint ITEP, 1993, N 97.
7. N.Gorbunov e.a. MES system for experimental data read-out and processing. Dubna. Preprint JINR, 1985, N P10-85-955.
8. D.von Harrach e.a. Proposal A4/1-93 to the MAMI PAC "Measurement of Parity Violating Electron Scattering on Hydrogen", Mainz Univ., 1993.